*Research Article*

# Research and Analysis on the Influence of Small Clear Distance Drilling and Blasting Method on the Existing Tunnel Structure

**Haibin Huang,**[1] **Peng Li,**[1] **Chuang Wang,**[1] **Bingxiang Yuan** ⓘ**,**[2] **Minjie Chen** ⓘ**,**[2] **and Weimin Feng**[2]

[1]*Zhuhai Dahengqin Co., Ltd., Guangzhou 519000, Zhuhai, China*
[2]*School of Civil and Transportation Engineering, Guangdong University of Technology, Guangdong 510006, Guangzhou, China*

Correspondence should be addressed to Bingxiang Yuan; yuanbx@gdut.edu.cn

In order to study the vibration influence of tunnel drilling and blasting method on the built tunnel with small clear distance, taking the intersection of Zhuhai Dahengqinshan No. 1 tunnel and Zhuji urban rail tunnel as the engineering background, we used ABAQUS finite element software to conduct numerical simulation analysis on the influence of different blasting loads on existing tunnels with small clear distance in Zhuji tunnel construction. The following conclusions were drawn: the blasting construction of the tunnel under construction had the greatest impact on the vault of the existing tunnel; when the peak load was reduced by half, the stress value, vertical displacement, and resultant velocity of Mises were also reduced by half, which indicates that reducing the peak value of blasting load appropriately can ensure the safety of tunnel construction. When the peak load is 2.7 MPa, the measured and simulated values were less than the resultant velocity limit required by the specification. In addition, the relative error between the measured value and the simulated value was less than 5%, indicating the accuracy of the numerical simulation.

## 1. Introduction

With the continuous development of urban subway network, the utilization scale of urban underground space is also gradually expanding. In the limited underground space, the construction of small spacing tunnel has obvious advantages and plays a positive role in tunnel construction [1–3]. At present, drilling and blasting method is mostly used in small spacing tunnel construction in China [4, 5]. If the distance between the tunnels is too small, the construction of the tunnel drilling and blasting method will inevitably affect the structural safety of the existing tunnel, disturb the surrounding rock, and then cause a series of environmental diseases of the surrounding buildings [6–8]. Therefore, great attention should be paid to the influence of drilling and blasting construction on the existing tunnel structure.

At present, domestic and foreign scholars have done some research on vibration caused by tunnel drilling and blasting construction. Wang et al. [9] recorded and analyzed the field monitoring data of a tunnel blasting and concluded

that when the main frequency of blasting vibration through the tunnel is less than 50 Hz, the existing highway roads will not produce resonance. Hao et al. [10] used LS-DYNA to discuss the changes of vibration velocity and equivalent stress of the surrounding rock caused by different clearance under blasting. It is found that the larger the clearance, the lesser the disturbance of the surrounding rock and the faster the attenuation of the vibration velocity of the existing tunnel. Luan et al. [11] relied on the Mongolian road tunnel project and used the finite element software to obtain the result that, in the blasting construction of large section tunnel, the radial vibration velocity of the support structure of the early excavated tunnel is greater than the vertical and tangential vibration velocity.

The geological condition of Zhuhai Dahengqinshan Tunnel project is poor, and the vertical clear distance between the two tunnels is small (the minimum clear distance is 3.5 m). The drilling and blasting construction of the Zhuji tunnel will cause disturbance to Dahengqinshan Tunnel. Therefore, it is necessary to improve the design scheme through numerical simulation to ensure the safety of tunnel

structure and surrounding buildings in the construction process of the Zhuji tunnel step method [12–14].

In this study, taking the intersection of Zhuhai dahengqinshan No. 1 tunnel and Zhuji urban rail tunnel as the engineering background, we used the ABAQUS finite element software to compare with the field monitoring data. This study systematically studied the influence of different blasting loads on the existing tunnel structure with a small clear distance.

## 2. Engineering Overview and Field Monitoring

### 2.1. Overview of Engineering Example.
The Dahengqinshan Tunnel is located in Hengqin new area of Zhuhai City. It is one of the "aorta" of Hengqin Island. This section of tunnel is underneath the planned Zhuji urban rail tunnel on the right line YK1 + 281 and the left line ZK1 + 289, with a buried depth of about 100 m. The minimum vertical clearance between two tunnels is 3.5 m, and the position plane relation of the two tunnels is shown in Figure 1. The design standard of Dahengqinshan No. 1 tunnel is 60 km/h, which is a two-way 6-lane municipal tunnel of urban main road. The tunnel is constructed by spray anchor support, composite lining, and CRD method. The design standard of the Zhuji urban rail tunnel is 160 km/h double-track intercity railway, which is constructed by the step method.

### 2.2. Field Monitoring Projects.
Because the blasting excavation of the Zhuji tunnel will cause the segment deformation of Hengqinshan Tunnel, which has a great influence on the stress change of the surrounding rock, reliable monitoring methods are needed to ensure personnel safety and tunnel construction efficiency. According to the engineering geological report and the construction characteristics of CRD method, the monitoring items of vault subsidence, arch foot displacement, and blasting vibration on the left line of Dahengqinshan Tunnel in cross section are set up (Figure 2).

## 3. Model Establishment

### 3.1. Model Simplification and Material Parameters.
The construction conditions simulated in this study are as follows: after the second lining construction of Dahengqinshan Tunnel, which is a built tunnel, Zhuji urban rail tunnel passes through as a new tunnel. Using ABAQUS finite element software, based on the survey data of Dahengqinshan project and BIM model data, we establish a three-dimensional geological model to generate rock mass element. The model in this study is 240 m long, 100 m wide, and 135 m high (Figure 3). In Figure 3, the lower side is the Dahengqinshan double-track tunnel, and the upper side is the Zhuji tunnel. As some tunnel sections of Dahengqinshan No. 1 tunnel include SD2 and SD3 sections, and according to the project data, part of SD1 section is far away from the overlapping intersection of the two tunnels, and the impact is far less than the overlapping intersection; Dahengqinshan Tunnel is simplified to only SD2 and SD3 sections in this simulation. Considering that the influence of elevation

difference caused by tunnel slope on the calculation is also quite small, the model is simplified with no slope. On the other hand, due to the buried depth of the Hengqinshan Tunnel, considering the influence range of the tunnel construction and the fact that the surface is undulating but basically on the same horizontal plane, the top of the model is simplified to a plane. In ABAQUS modeling and calculation, the tunnel lining adopts plate shell element and C35 concrete material, which is calculated according to the elastic constitutive model, and the soil around the tunnel adopts solid element and the modified Mohr–Coulomb model. According to the results of field tests and investigation reports, the specific material parameters of the model are shown in Table 1.

### 3.2. Boundary Condition.
After analysis, the soil adopts tetrahedral elements with 1380685 grids and 30851 elements in total. The model grid diagram is shown in Figure 4. In the simulation process, the tectonic stress of soil is not considered, and only the self-weight of soil is considered as the initial ground stress. Constraints in three directions are imposed on the bottom surface of the model, and displacement constraints in the normal direction of the corresponding surface are imposed on the model side. The role of constraints is to make the constraints on the model area consistent with the actual rock-soil interaction.

### 3.3. Explosive Load.
In this study, the triangular load model [15–17] is selected to simulate the influence of blasting stress wave on the surrounding rock. The pressure load changing with time is applied along the wall of the Zhuji urban rail tunnel to simulate the impact caused by blasting. The load loading diagram and load curve diagram are shown in Figures 5 and 6 respectively.

The peak value of explosive load is determined by explosive density, explosive velocity, explosive roll diameter, and hole diameter. According to the theoretical calculation method [18], the peak value of blast hole under the condition of noncoupling charge is calculated according to the following equation:

$$P_b = \frac{1}{8}\rho_0 D^2 \left(\frac{R_c}{R_b}\right), \tag{1}$$

where $P_b$ is the peak pressure of blast hole, $\rho_0$ is the explosive density, $D$ is the detonation velocity of explosive, $R_c$ and $R_b$ are the radius of charge roll and blast hole respectively, $\eta$ is the increasing multiple of the collision between explosive gas and hole wall, and its value range is $\eta = 8 \sim 11$.

According to reference [18–20], the pressure load formula equivalent to the pressure load on the centerline of blast hole is

$$P_e = \left(\frac{2r_0}{a}\right)P_b, \tag{2}$$

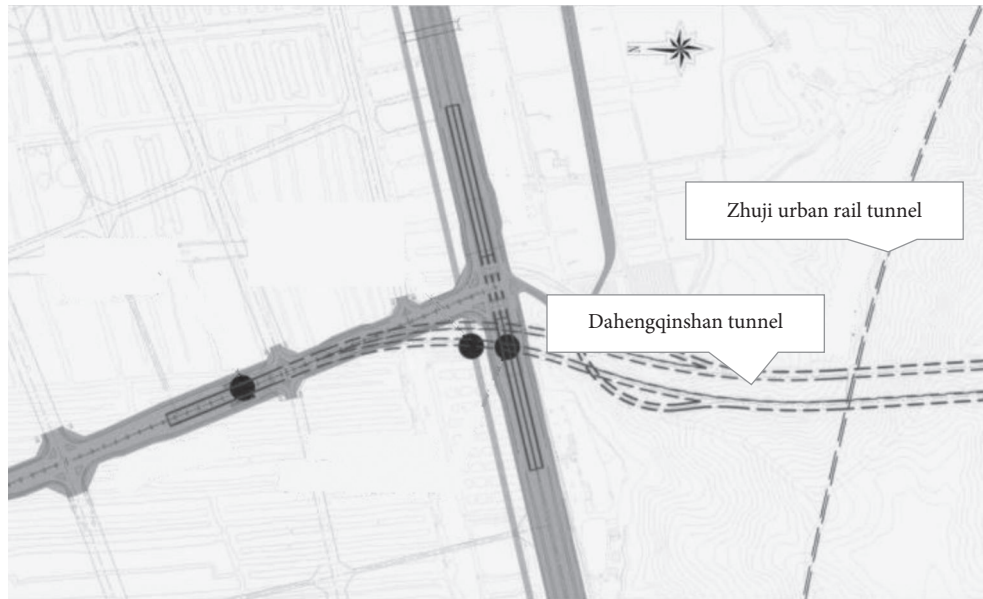where $P_e$ is the equivalent pressure, $r_0$ is the hole radius, and $a$ is the hole spacing.

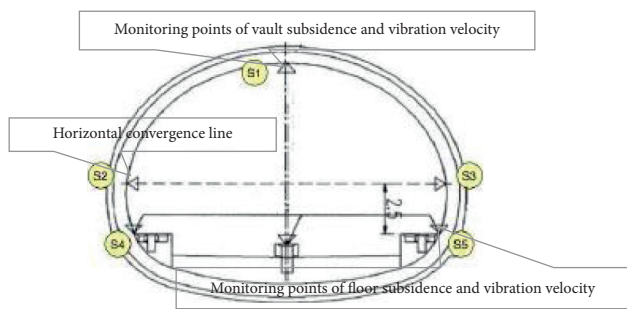Figure 1: Plane relation diagram of tunnel position.



Figure 2: Layout of displacement measuring points on the left line of Dahengqinshan Tunnel.
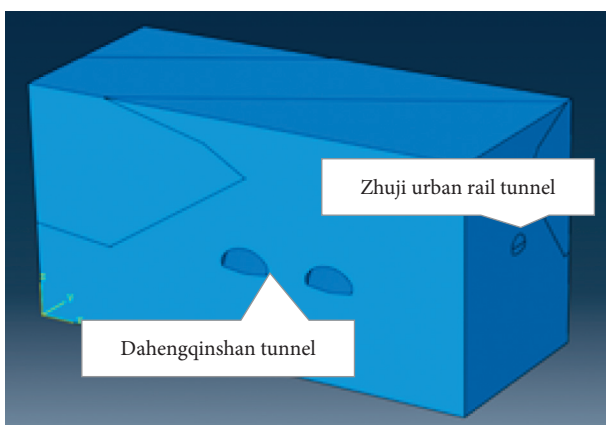


Figure 3: Overview of the tunnel model.

## 4. Influence Analysis of Blasting Peak Load

*4.1. Selection of Monitoring Points and Excavation Sections.* In order to determine the maximum impact effect on the tunnel, monitoring points are arranged on a section (ZK1 + 252) of the left line of Dahengqinshan Tunnel directly below the Zhuji urban rail tunnel. Five monitoring points are arranged at the vault, left arch waist, right arch waist, left arch foot, and right arch foot on ZK1 + 252 section, with numbers of 9851, 1108, 970, 191, and 487 respectively. Figure 7 shows the location of monitoring points and the direction of tunnel excavation.

In tunnel construction, it is generally believed that, within the range of 3–5 times of tunnel diameter, the influence of tunnel construction is quite obvious, and it can be considered that the construction has little impact on the surrounding environment beyond the range of 3–5 times the tunnel diameter [21, 22]. Therefore, as shown in Figure 8, the Zhuji urban rail tunnel is divided into 16 sections from left to right in the *X* direction. The excavation depth of each section is 15 m, and the total length of the Zhuji urban rail tunnel is 240 m. The 16 sections correspond to the excavation depth of the Zhuji tunnel in turn: 15 m, 30 m, 45 m, 60 m, 75 m, 90 m, 105 m, 120 m, 135 m, 150 m, 165 m, 180 m, 195 m, 210 m, 225 m, and 240 m, so as to analyze the impact of drilling and blasting construction of the Zhuji urban rail tunnel on the left line of Dahengqinshan Tunnel. This section analyzes the dynamic influence of the continuous excavation of the Zhuji tunnel under the peak load of 5 MPa and 10 MPa on the left line structure of Dahengqinshan Tunnel.

*4.2. Tunnel Construction Process*

(1) The first analysis step: the soil layer was established, the soil layer parameters were given, the boundary conditions, were imposed, and then the initial in situ stress balance was carried out.

(2) According to 16 sections, the excavation of each section of the Zhuji tunnel corresponds to one analysis step, with a total of 17 steps.

TABLE 1: Material parameters.

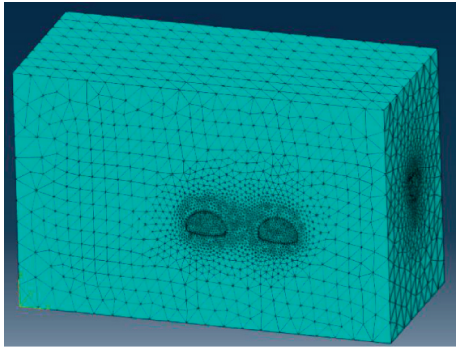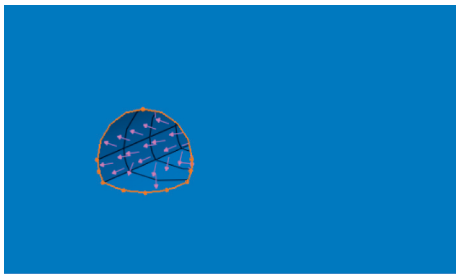| Name of soil layer | Volumetric weight (kN/m³) | Constitutive model | Elastic modulus (GPa) | Poisson ratio | Friction angle (°) | Cohesion (MPa) |
|---|---|---|---|---|---|---|
| Granite fracture zone | 25.6 | Modified Mohr–Coulomb | 2.3 | 0.25 | 30 | 22 |
| Moderately weathered granite | 25.6 | Modified Moore–Coulomb | 4.72 | 0.19 | 37 | 35 |
| C35 concrete | 24 | Linear elasticity | 31.5 | 0.19 | - | - |



FIGURE 4: Model grid diagram.
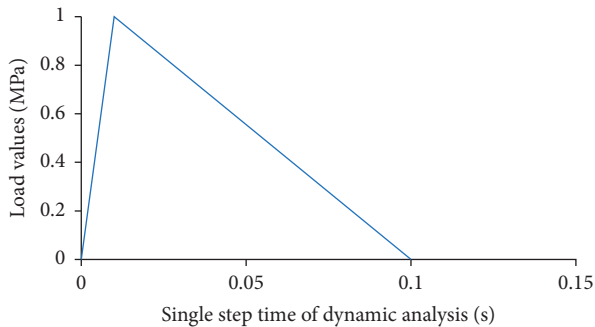


FIGURE 5: Schematic diagram of load loading.



FIGURE 6: Schematic diagram of load curve.

(3) When the function of making the element disappear is to be realized, ABAQUS software will multiply the corresponding part of the overall stiffness matrix by a fairly small coefficient, and the mass, stress, strain, damping, and output element load will also be zero. "Activation" is to realize the reappearance effect of the element by changing the stiffness of the element
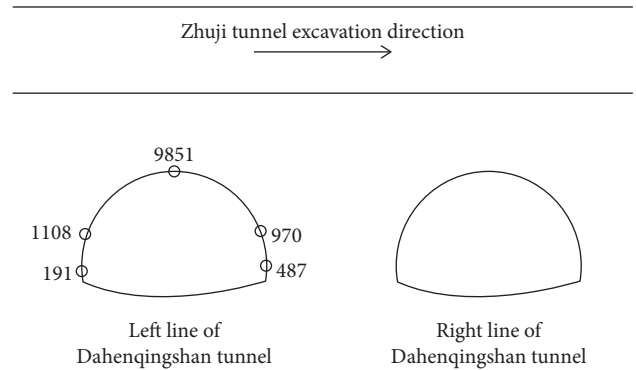
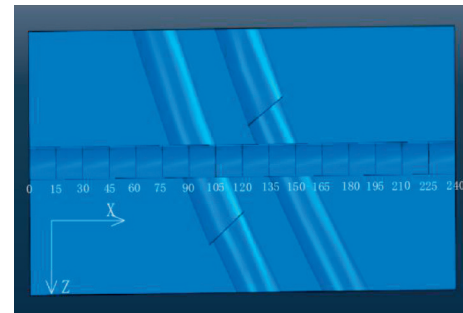

FIGURE 7: Corresponding position of point number.



FIGURE 8: Schematic diagram of tunnel excavation direction and depth.

in the whole. Using this method, the process simulation of tunnel excavation can be realized.

### 4.3. Numerical Simulation Results

(1) When the peak load is 10 MPa, the relationship between the excavation depth of the Zhuji tunnel and the Mises stress, and vertical displacement and blasting speed of each monitoring point is shown in Figure 9. In Figure 9(a), the peak stress of Mises at the vault is the largest, which is 34 MPa, corresponding to the monitoring point 9851. The peak stress of the arch foot on both sides is the second, corresponding to the monitoring point 191 and the monitoring point 478, and the peak stress is 18 MPa and 12 MPa, respectively. As shown in Figure 9(b), the maximum vertical displacement of the arch vault
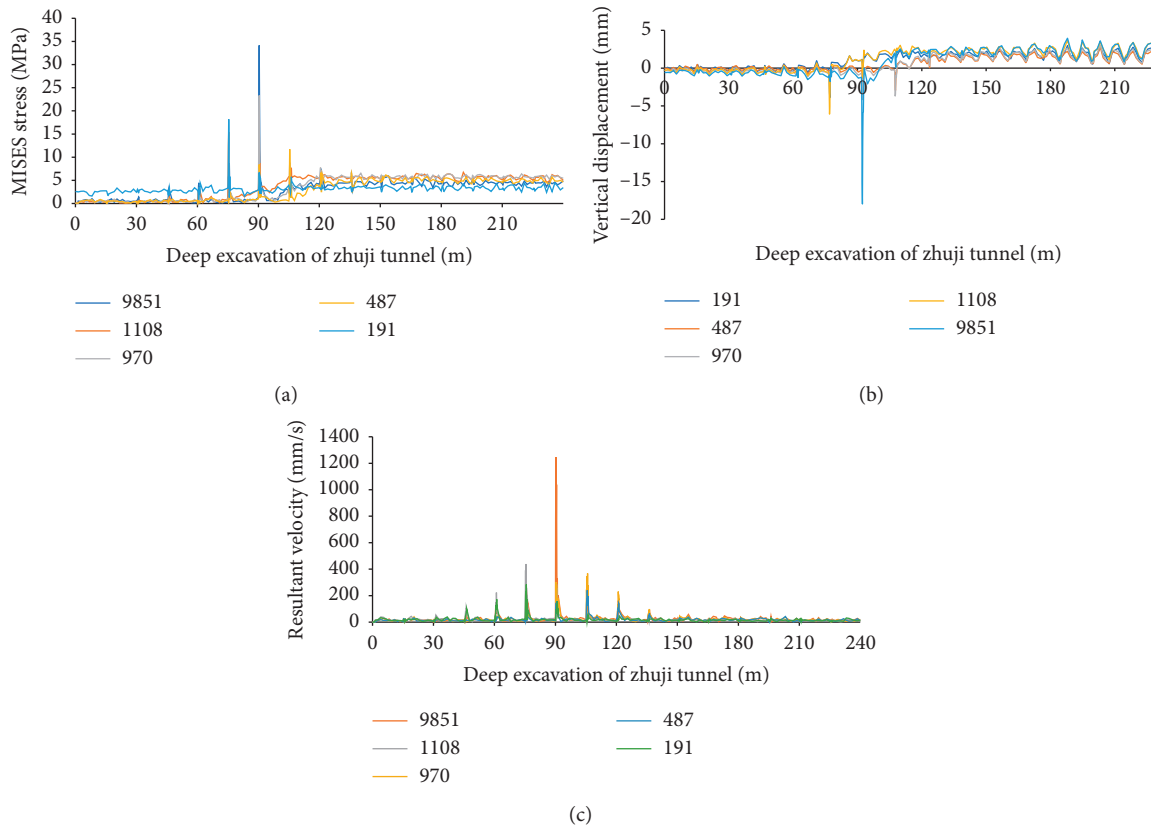
FIGURE 9: Numerical simulation results under 10 MPa peak load. (a) Mises stress excavation-excavation depth curve. (b) Vertical displacement-excavation depth curve. (c) Resultant velocity-excavation depth curve.

is 18 mm. The maximum vertical displacement measured at the left arch waist monitoring point 1108 is 6 mm, and the right arch waist monitoring point 970 is 3.7 mm. The displacement direction is downward.

As for the speed of each section, it can be seen from Figure 9(c) that the speed measured at the monitoring point 9851 on the top of the tunnel at the excavation depth of 90 m is the largest, reaching 1246 mm/s. The peak velocities measured by the monitoring points 970 and 1108 at the left and right arch waists are also quite high, which are 368 mm/s and 439 mm/s respectively.

(2) When the peak load is 5 MPa, the calculation results are shown in Figure 10. Similar to the calculation results of peak load of 10 MPa, the maximum stress peak value measured at the top monitoring point of tunnel is 16.7 MPa (Figure 10(a)). The results measured at monitoring point 970 are the second, and the peak stress is 12 MPa. The Mises stress value of each monitoring point after excavation is relatively stable, and its value is between 4 and 6 MPa. As shown in Figure 10(b), the maximum displacement peak is monitoring point 9851, which is 9.3 mm, and the larger value point is 1108, which is 3 mm.

For the speed of each section, the maximum velocity peak is monitoring point 9851, the value is 625 mm/s,

followed by two monitoring points 970 and 1108, and the values are 184 mm/s and 220 mm/s.

*4.4. Analysis.* Compared with Figures 9 and 10, it can be seen that the peak load of 5 MPa graphic trend is basically consistent with 10 MPa. When the blasting peak load is reduced from 10 MPa to 5 MPa, the Mises stress at the vault is reduced by 51%, the vertical displacement is reduced by 48%, and the maximum resultant velocity is reduced by 50%. The vertical displacement and maximum velocity of the left arch waist are reduced by 50%, and the right arch waist is also reduced by 50%. When the peak load is reduced by half, the maximum Mises stress peak, vertical displacement, and resultant velocity are basically reduced by half. It can be seen that the value of the peak load has a great influence on the existing tunnel. By reducing the peak load of blasting appropriately, we can ensure the safety of the existing tunnel and the construction efficiency of the tunnel under construction.

Combined with the analysis of the numerical simulation results, the Mises stress value, vertical displacement, and resultant velocity all reached the peak value at the excavation depth of 90 m in the Zhuji tunnel. This is because when the excavation depth reaches 90 m, Zhuji urban rail tunnel is closest to the left line of Dahengqinshan, which has the greatest disturbance to the existing tunnel. Before the excavation depth of 90 m, the vertical deformation of each
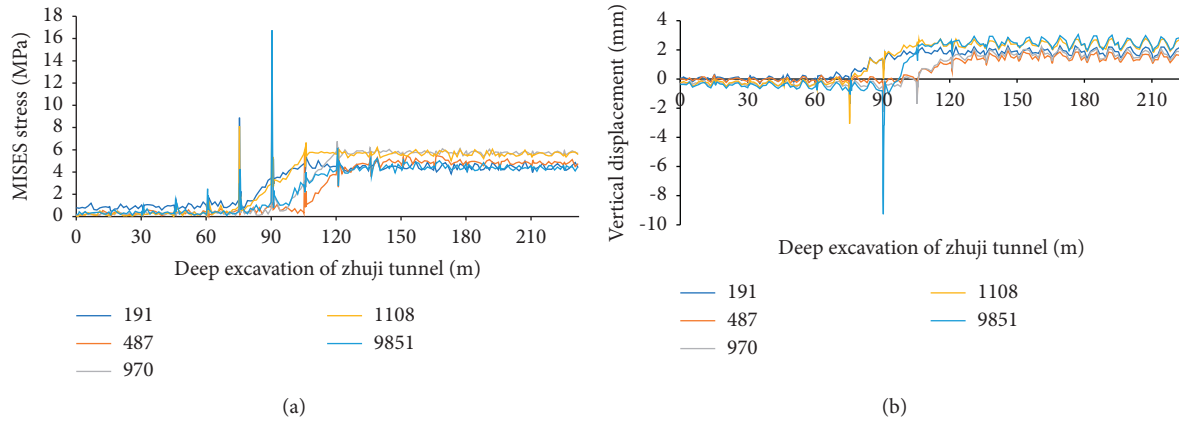
(a)

(b)

FIGURE 10: Numerical simulation results under 10 MPa peak load. (a) Mises stress excavation-excavation depth curve. (b) Vertical displacement-excavation depth curve.

point is settlement and increases with the increase of excavation depth. After 90 m, with the increase of excavation depth, each measuring point shows uplift and then tends to be stable. This is because the upper tunnel has been far away from the left line of the existing tunnel and constructed above the right line. At this time, the data of each measuring point of the right line tunnel are the same as the vertical deformation of the left line before the excavation depth of 90 m, which is manifested as settlement. Due to stratum loss, the left line tunnel bulges at this time. In addition, when the excavation depth is 60 m to 180 m in the middle section, the dynamic effect is more obvious.

## 5. Application Research

It can be seen from partial explosive parameters in Table 2 that when the ratio of cartridge to blast hole is 0.5, the peak value of equivalent load can be calculated as 2.7 MPa by equations (1) and (2).

Under the influence of blasting construction of small clear distance tunnel, the existing tunnel will produce vibration, and the vibration velocity is the main parameter to analyze and evaluate the dynamic influence [23–25].

In the numerical simulation analysis of this study, the vibration velocity corresponds to the resultant velocity in the output results. The resultant velocity is a scalar whose value is the vector sum of the velocities in three directions. According to the specification [26–28] and the engineering data of the Hengqinshan Tunnel project, the maximum vibration velocity of the tunnel is required to be 15 cm/s.

Therefore, the main purpose of this study is to calculate the maximum vibration velocity corresponding to each excavation section during the excavation of Dahengqinshan Tunnel passing through the existing tunnel. And we compare it with the maximum vibration velocity vibration value required by the specification, so as to simulate whether the vibration of the existing tunnel during the construction of small spacing drilling and blasting method meets the engineering requirements. As shown in Table 3, we select and analyze the resultant velocity values of each measuring point

corresponding to the five excavation depths that have the greatest impact on the left line of Dahengqinshan Tunnel.

It can be seen from Table 3 that the monitoring points at different positions of the tunnel section have different maximum resultant velocity values during the process of the Zhuji urban rail tunnel crossing above the left line of the Dahengqinshan Tunnel. The maximum resultant velocity calculated by the measuring point 9851 at the vault is 11.28 cm/s, which is greater than the other four measuring points. The resultant velocity of the five measuring points on the cross section reaches the peak under different excavation depths of the Zhuji tunnel. Among them, the measuring point 9851 reached the peak at the depth of 78 m, and then the Zhuji tunnel continued to be excavated. With the increase of excavation depth, the closing speed at the vault decreased [29–31]. The simulated resultant velocity of the left arch waist measuring point 1108 and the left arch foot measuring point 191 reaches the maximum at the depth of 60 m of tunnel excavation, which are 2.54 cm/s and 3.91 cm/s, respectively. The maximum velocity of the right arch waist 970 is 3.49 cm/s, which is obtained at the excavation depth of 84 m. The right arch foot measuring point 487 reaches the maximum speed of 1.97 cm/s at the excavation depth of 90 m.

The resultant velocity of the measuring point 9851 at vault under different excavation depths is greater than that of the other four measuring points [32, 33]. This is because the stress wave caused by the blasting load of the tunnel will continue to decay along the distance in the process of transmission in the rock stratum, and the distance from the vault to the tunnel is shorter than that from the arch waist and arch foot to the tunnel. Similarly, the resultant velocity of measuring points 1108 and 970 located at arch waist is larger than that of measuring points at the arch foot, which is also because the distance from the stress wave to the arch waist is shorter than that to the arch foot. Compared with the speed limit of 15 cm/s given above, the simulation values of each monitoring point on the left line are less than 15 cm/s. So it is more appropriate to use the peak load of 2.7 MPa for construction.

Therefore, the construction of the Zhuji urban rail tunnel has the greatest impact on the vault of the left line section

TABLE 2: Partial explosive parameters.

| Name of explosive | Cartridge diameter (mm) | Explosive density (g/cm$^3$) | Explosive detonation velocity (m/s) |
|---|---|---|---|
| EL-102 emulsion oil | 20 | 1.05 | 3500 |
| No. 2 rock explosive | 22 | 1.1 | 2100~3000 |
| No. 3 rock explosive | 22 | 1.0 | 1600~1800 |

TABLE 3: Maximum closing speed of each monitoring point.

| Excavation depth (m) | Resultant velocity (cm/s) | | | | |
|---|---|---|---|---|---|
| | 191 | 1108 | 9851 | 970 | 487 |
| 54 | 2.27 | 3.87 | 1.68 | 0.49 | 0.35 |
| 60 | 2.54 | 3.91 | 3.61 | 0.83 | 0.35 |
| 78 | 1.39 | 2.94 | 11.28 | 3.11 | 1.15 |
| 84 | 0.82 | 1.78 | 10.72 | 3.49 | 1.67 |
| 90 | 0.68 | 1.29 | 5.89 | 3.31 | 1.97 |
| Maximum | 2.54 | 3.91 | 11.28 | 3.49 | 1.97 |

TABLE 4: Maximum vibration velocity component of monitoring points at tunnel vault.

| Monitoring location | Vibration (cm/s) | | |
|---|---|---|---|
| | X direction | Y direction | Z direction |
| Vault (ZK1 + 252) | 8.17 | 4.73 | 6.85 |

(ZK1 + 252) of Dahengqinshan Tunnel. The maximum value of vibration velocity in the field monitoring data of the monitoring point at the vault of this section is sorted out in Table 4. It can be seen that the relative error between the field monitoring data and the numerical simulation results at the vault is less than 5%, and the monitoring results of the actual project are less than the vibration velocity limit (15 cm/s) required by the specification, which can be in good agreement. It shows that the numerical simulation is more accurate and can reflect the vibration rate distribution law of different locations of the existing tunnel structure in the construction of small spacing tunnel drilling and blasting method. Taking the numerical simulation results of finite element software as the reference value, the safety accident prevention of tunnel overlapping cross section can be greatly improved.

## 6. Conclusions

Based on the Zhuhai Dahengqinshan No. 1 tunnel and Zhuji urban rail tunnel project, according to the field investigation results, this study used ABAQUS finite element software to simulate the tunnel drilling and blasting construction and systematically studied the influence of the existing tunnel structure caused by the blasting peak load. After a comprehensive analysis, the following main conclusions are as follows:

(1) The blasting peak load has different effects on the measuring points in different parts of the tunnel structure, and the blasting of the tunnel under construction has the greatest influence on the vault of the existing tunnel section.

(2) When the blasting peak load is reduced from 10 MPa to 5 MPa, the Mises stress, vertical displacement, and resultant velocity of each measuring point on the left section of Dahengqinshan Tunnel (ZK1 + 252) are basically reduced by half.

(3) The Mises stress value, vertical displacement, and combined velocity of each measuring point reached the peak at 90 m depth of Zhuji tunnel excavation and then decreased and stabilized with the increase of excavation depth.

(4) When the peak load is 2.7 MPa, the measured value and the simulated value are less than the speed limit (15 cm/s) required by the specification, and the relative error between the measured value and the simulated value is less than 5%. It is appropriate to use the load peak of 2.7 MPa for construction.

## Data Availability

The data used to support the findings of this study are available from the corresponding author upon request.

## Conflicts of Interest

The authors declare that they have no conflicts of interest regarding the publication of this study.

## Acknowledgments

## References

[1] J. Wang, F. Wu, and D. Qiu, "Construction technology and development prospect of underground space in China," *Architectural Technology*, vol. 49, no. 6, pp. 578–580, 2018.

[2] Q.C Zhang, Z. Dai, and Y. Shi, "Key technologies of new tunnel close crossing existing metro tunnel," *Journal of railway engineering*, vol. 37, no. 6, pp. 58–63, 2020.

[3] X. Jia, F. Xin, and J. Zheng, "Study on design and construction technology of small clear distance parallel stacked mine tunnel," *Urban rapid rail transit*, vol. 34, no. 5, pp. 111–118, 2021.

[4] J. Li, "Key technologies of tunnel excavation and support by drilling and blasting method," *China highway*, vol. 11, pp. 87–89, 2020.

[5] C. Zhang, X. Zhu, and S. Peng, "Key technologies for construction of small clear distance mining tunnel under existing buildings," *Sichuan architecture*, vol. 41, no. 3, pp. 229–231, 2021.

[6] X. Wang, W. Wang, and D. Du, "Study on fluid structure coupling of small clear distance interchange tunnel," *Journal of disaster prevention and mitigation engineering*, vol. 38, no. 4, pp. 700–708, 2018.

[7] Ji. Ling, C. Zhou, S. Lu, N. Jiang, and H. Li, "Modeling study of cumulative damage effects and safety criterion of surrounding rock under multiple full-face blasting of a large cross-section tunnel," *International Journal of Rock Mechanics and Mining Sciences*, vol. 147, 2021.

[8] H. Wang, Y. Wang, M. Wang, and Q. Zong, "Numerical analysis of the influence of foundation pit blasting on a nearby metro tunnel," *Shock and Vibration*, vol. 2021, Article ID 5585726, 15 pages, 2021.

[9] R. Wang, D. Yuan, F. Dang et al., "Influence scope of blasting vibration for construction of new tunnel undercrossing existing roads," *Rehabilitation Medicine*, vol. 34, no. 3, pp. 238–244, 2017.

[10] H. Ruijun, "Dynamic response analysis of small clear distance tunnel under blasting load," *Water resources and hydropower technology*, vol. 51, no. S2, pp. 291–297, 2020.

[11] L. Guitao, Z. Wang, Z. Song, and H. Yu, "Analysis of the influence of lately excavated tunnel blasting on the vibration of early excavated tunnel in small-space tunnel," *IOP Conference Series: Earth and Environmental Science*, vol. 643, no. 1, Article ID 012025, 2021.

[12] B. Bai, G. Yang, and G. Yang, "A thermodynamic constitutive model with temperature effect based on particle rearrangement for geomaterials," *Mechanics of Materials*, vol. 139, Article ID 103180, 2019.

[13] B. Yuan, M. Sun, L. Xiong, Q. Luo, S. P. Pradhan, and H. Li, "Investigation of 3D deformation of transparent soil around a laterally loaded pile based on a hydraulic gradient model test," *Journal of Building Engineering*, vol. 28, no. 3, Article ID 1010124, 2020.

[14] X. Que, Z. Zhu, and W. Lu, "Anisotropic constitutive model of pentagonal prism columnar jointed rock mass," *Bulletin of Engineering Geology and the Environment*, vol. 79, no. 1, pp. 269–286, 2020.

[15] M. Sheng, Y. Yao, and J. Sun, "Experimental study on far zone explosion load of blast hole during borehole blasting," *Blasting*, vol. 36, no. 3, pp. 1–8, 2019.

[16] X. Que, Z. Zhu, Z. Niu, and W. Lu, "Estimating the strength and deformation of columnar jointed rock mass based on physical model test," *Bulletin of Engineering Geology and the Environment*, vol. 80, no. 2, pp. 1557–1570, 2021.

[17] S. Luo, Y. Peng, and W. Lu, "Numerical simulation of blasting damage and damage mechanism in deep tunnel excavation," *Journal of rock mechanics and engineering*, vol. 40, no. S1, pp. 2760–2772, 2021.

[18] L. Tao, *Urban Underground Engineering*, Science Press, Beijing, China, 2011.

[19] B. Bai, D. Rao, T. Chang, and Z. Guo, "A nonlinear attachment-detachment model with adsorption hysteresis for suspension-colloidal transport in porous media," *Journal of Hydrology*, vol. 578, Article ID 124080, 2019.

[20] C. Cui, K. Meng, C. Xu, Z. Liang, H. Li, and H. Pei, "Analytical solution for longitudinal vibration of a floating pile in saturated porous media based on a fictitious saturated soil pile model," *Computers and Geotechnics*, vol. 131, Article ID 103942, 2021.

[21] L. Wang, Li Xiang, F. Guo, S. Tang, X. Lu, and A. Hanif, "Influence of reactivity and dosage of MgO expansive agent on shrinkage and crack resistance of face slab concrete," *Cement and Concrete Composites*, vol. 2022, Article ID 104333, 2021.

[22] J. Xiao, W. Qu, H. Jiang, L. Li, J. Huang, and L. Chen, "Fractal characterization and mechanical behavior of pile-soil interface subjected to sulfuric acid," *Fractals - Complex Geometry, Patterns, and Scaling in Nature and Society*, vol. 29, no. 2, Article ID 2140010, 2021.

[23] I. D. Isaac and C. T. T. Bubb, "Engineering aspects of underground cavern excavation at Dinorwic - Part 3. A study of blast vibrations, Part 1," *International Journal of Rock Mechanics and Mining Sciences & Geomechanics Abstracts*, vol. 18, no. 6, 1981.

[24] B. Yuan, Z. Li, Z Su, Q. Luo, M. Chen, and Z. Zhao, "Sensitivity of multistage fill slope based on finite element model," *Advances in Civil Engineering*, vol. 2021, Article ID 6622936, 13 pages, 2021.

[25] B. Bai, R. Zhou, G. Cai, W. Hu, and G. Yang, "Coupled thermo-hydro-mechanical mechanism in view of the soil particle rearrangement of granular thermodynamics," *Computers and Geotechnics*, vol. 137, no. 8, Article ID 104272, 2021.

[26] Y. Wu, J. Cui, J. Huang, W. Zhang, N. Yoshimoto, and L. Wen, "Correlation of critical state strength properties with particle shape and surface fractal dimension of clinker ash," *International Journal of Geomechanics*, vol. 21, no. 6, Article ID 04021071, 2021.

[27] GB 6722-2014, *Safety Regulations for Blasting*, State Standardization Publishing House, Beijing, China, 2014.

[28] B. Yuan, Z. Li, Z. Zhao, H. Ni, Z. Su, and Z. Li, "Experimental study of displacement field of layered soils surrounding laterally loaded pile based on Transparent Soil," *Journal of Soils and Sediments*, vol. 21, no. 9, pp. 3072–3083, 2021.

[29] K. Meng, C. Cui, Z. Liang, H. Li, and H. Pei, "A new approach for longitudinal vibration of a large-diameter floating pipe pile in visco-elastic soil considering the three-dimensional wave effects," *Computers and Geotechnics*, vol. 128, Article ID 103840, 2020.

[30] B. Yuan, Z. Li, Y. Chen et al., "Mechanical and microstructural properties of recycling granite residual soil reinforced with glass fiber and liquid-modified polyvinyl alcohol polymer," *Chemosphere*, vol. 268, Article ID 131652, 2021.

[31] B. Bai, Q. Nie, X. Wang, and W. Hu, "Cotransport of heavy metals and SiO2 particles at different temperatures by seepage," *Journal of Hydrology*, vol. 597, Article ID 125771, 2021.

[32] B. Yuan, C. Rui, G. Deng, T. Peng, Q. Luo, and X. Yang, "Accuracy of interpretation methods for deriving p–y curves from model pile tests in layered soils," *ASTM Journal of Testing and Evaluation*, vol. 45, no. 4, pp. 1238–1246, 2017.

[33] B. Yuan, M. Sun, Y. Wang, L. Zhai, Q. Luo, and X. Zhang, "Full 3D displacement measuring system for 3D displacement field of soil around a laterally loaded pile in transparent soil," *International Journal of Geomechanics*, vol. 19, no. 5, Article ID 04019028, 2019.